MATERIALS CHEMISTRY FRONTIERS

RESEARCH ARTICLE

View Article Online
View Journal | View Issue

Cite this: *Mater. Chem. Front.*, 2024, **8**, 1120

Multiplying the electroluminescence efficiencies of red TADF emitters *via* a regioisomeric approach of the donor unit†

Xi Zhang,[a] Hui Wang,[a] Jia-Xiong Chen,[b] Lu Zhou,[a] Xiao-Yao Hao,[a] Jia Yu,[a] Kai Wang *[ac] and Xiao-Hong Zhang *[ad]

Received 31st October 2023,
Accepted 15th December 2023

DOI: 10.1039/d3qm01170d

rsc.li/frontiers-materials

A regioisomeric strategy is of great significance to the design of molecules with red thermally activated delayed fluorescence (TADF); however, previous studies have mainly focused on the regioisomerism of acceptor frameworks. Herein, we propose a donor-induced regioisomeric strategy for developing red TADF emitters for the first time. Intriguingly, DPDPZ-PXZPh, with 3-position connected 10-phenyl-10*H*-phenoxazine (PhPXZ) as the donor exhibits a faster radiative rate, lower reorganization energies, and a superior photoluminescence quantum yield compared with the control compound DPDPZ-PhPXZ containing a 14-position connected PhPXZ. The corresponding organic light-emitting diode (OLED) based on DPDPZ-PXZPh not only achieves an evidently redshifted emission peaking at 600 nm but also delivers a much-improved external quantum efficiency of 28.0%, which is a nearly 1.6-fold efficiency enhancement relative to the DPDPZ-PhPXZ-based device (17.8%). This result demonstrates the important role of donor linking engineering in constructing high-performance red TADF emitters, offering a new isomeric pattern for developing high-efficiency red OLEDs.

Introduction

Metal-free emitters of thermally activated delayed fluorescence (TADF) are capable of utilizing all electronically generated excitons for emission (*i.e.*, 100% internal quantum efficiency) and are promising alternatives for noble metal-containing phosphorescence emitters in commercial organic light-emitting diodes (OLEDs).[1–4] Donor (D)–acceptor (A)-type molecular structures are the most adopted molecular design strategy to construct TADF emitters, in which reverse intersystem crossing (RISC) from triplet to singlet excitons can be facilely activated by sufficiently restricting the highest occupied molecular orbital (HOMO) to D segments and the lowest unoccupied molecular orbital (LUMO) to A segments, respectively.[5–9] Along this line, high-performance blue and green TADF emitters have flourished; in contrast, progress in efficient red TADF emitters is lagging far behind.[10,11] A chief culprit is the energy-gap law, that is, the nonradiative rate (k_{IC}) *via* the internal conversion (IC) channel will be exponentially magnified as optical energy gaps linearly decrease.[12,13] Thus, without sufficiently fast rates (k_r) of radiative decay (*i.e.*, far surpassing k_{IC}), red TADF emitters would unavoidably suffer from low photoluminescence (PL) quantum yields (Φ_{PL}s) and thus lower device performance.[14,15]

To pursue full exciton harvesting of red TADF emitters, the currently employed A candidates are generally large π-fused frameworks that can suppress the nonradiative decays from the A aspect, and the D candidates are mostly either triphenylamine (TPA) and its derivatives, *i.e.*, flexible segments with mild D–A twists to enhance k_r or relatively rigid components, *e.g.*, phenoxazine (PXZ), with high D–A twists to minimize the nonradiative decays from the D aspect.[16–20] The diversity of D–A pairs for developing high-performance red TADF emitters is relatively limited. Regioisomeric strategies were thus explored to further tap the potential with limited D/A pairs, *i.e.*, employing the same D–A pairs but with different D–A linking modes.[21–25] Through such strategies, minor structural changes may lead to significant differences in photophysical behaviors and electroluminescence performance.[26–28] For example, Xu *et al.* demonstrated that moving TPA units from the *ortho*- to *para*-positions of an A framework brought about an approximately 90-fold enhancement in k_r, resulting in a higher Φ_{PL} and a

[a] *Institute of Functional Nano & Soft Materials (FUNSOM), Soochow University, Suzhou, Jiangsu 215123, P. R. China. E-mail: wkai@suda.edu.cn, xiaohong_zhang@suda.edu.cn*
[b] *School of Chemical Engineering and Light Industry, Guangdong University of Technology, Guangzhou, Guangdong, 510006, P. R. China*
[c] *Jiangsu Key Laboratory for Carbon-Based Functional Materials & Devices, Soochow University, Suzhou, 215123, Jiangsu, P. R. China*
[d] *Jiangsu Key Laboratory of Advanced Negative Carbon Technologies, Soochow University, Suzhou, 215123, Jiangsu, P. R. China*

† Electronic supplementary information (ESI) available. See DOI: https://doi.org/10.1039/d3qm01170d

state-of-the-art external quantum efficiency (EQE) of 12.3%.[29] Wang *et al.* reported a pair of isomeric red TADF emitters, where the TPA segment was attached at different sites on the A framework with a *trans*/*cis*-arrangement pattern. The resultant *trans*-isomer achieved an evidently increased Φ_{PL} and superior device efficiency compared to the *cis*-isomer.[30] Notably, previous studies have only focused on regioisomerism in the A framework, *i.e.*, attaching D units onto the different substitution sites on the A segment.[31–33] On the other hand, the attaching sites of the D segments are fixed in stereotype, *e.g.*, the linking site of PXZ is the N-position that can induce high D–A twist, and that of TPA is the *para*-position that ensures sufficient D–A conjugation (as seen in Fig. 1).[34,35] To the best of our knowledge, no studies have explored the regioisomerism in D components thus far, hindering the understanding and further development of high-performance red TADF emitters.

In this work, we thus designed and synthesized a pair of red TADF regioisomers, namely, 3-(11,12-di(pyridin-3-yl)dibenzo-[*a*,*c*]phenazin-3-yl)-10-phenyl-10*H*-phenoxazine (DPDPZ-PXZPh) and 10-(4-(11,12-di(pyridin-3-yl)dibenzo[*a*,*c*]phenazin-3-yl)phenyl)-10*H*-phenoxazine (DPDPZ-PhPXZ). Both compounds consist of an identical D/A pair, while their D–A linking positions at the D side are different (see their chemical structures in Fig. 1). DPDPZ-PhPXZ follows a conventional D–A linking mode, that is, the A framework links to the 14-position of 10-phenyl-10*H*-phenoxazine (PhPXZ), while for DPDPZ-PXZPh, the A framework links to its 3-position. Due to the milder D–A twist, DPDPZ-PXZPh exhibits higher oscillator strength (*f*), which brings about a higher k_r that sufficiently exceeds unwanted nonradiative energy dissipation, thus furnishing a higher Φ_{PL} of 95% with respect to DPDPZ-PhPXZ. Eventually, an optimized OLED based on DPDPZ-PXZPh achieves a redder emission peaking at 600 nm and a higher EQE of 28.0%, which is a nearly 1.6-fold enhancement compared to the DPDPZ-PhPXZ-based device (17.8%). This work not only demonstrates the feasibility of D-induced regioisomeric engineering for developing more advanced red TADF emitters but also provides new isomer insights into the construction of high-efficiency red TADF-OLEDs.

Results and discussion

Molecular design, synthesis and characterization

Herein, 11,12-di(pyridin-3-yl)dibenzo[*a*,*c*]phenazine (DPBPZ), a classical A segment, is employed as the A component due to its rigid and planar π-conjugated structure that can sufficiently suppress nonradiative decays[10] and links to PhPXZ, a D unit with suitable electron-donating ability and two different linking sites. For DPDPZ-PhPXZ, acting mainly as the control compound, the DPBPZ framework is linked at the 14-position of PhPXZ, that is, a conventional linking mode, while for DPDPZ-PXZPh, DPBPZ unconventionally attaches at the 3-position of PhPXZ. It is expected that by subtly modulating the linking modes of the D segment, various physical properties and key dynamics could be further modulated, helping to deepen the understanding of the structure–property relationships of red TADF emitters.

The synthetic procedures of DPDPZ-PXZPh and DPDPZ-PhPXZ are depicted in Scheme S1 (ESI†). Buchwald–Hartwig reactions were first carried out between 10-phenyl-3-(4,4,5,5-tetramethyl-1,3,2-dioxaborolan-2-yl)-10*H*-phenoxazine (M1)/10-(4-(4,4,5,5-tetramethyl-1,3,2-dioxaborolan-2-yl)phenyl)-10*H*-phenoxazine (M2) and 3-bromophenanthrene-9,10-dione to obtain the two intermediates, 3-(10-phenyl-10*H*-phenoxazin-3-yl)phenanthrene-9,10-dione (PhO-PXZPh) and 3-(4-(10*H*-phenoxazin-10-yl)phenyl)phenanthrene-9,10-dione (PhO-PhPXZ). Then, two target materials were obtained *via* cyclization reactions between the above intermediates and 4,5-di(pyridin-3-yl)benzene-1,2-diamine, which can be synthesized according to our previously reported methods.[10] The chemical structures of all the intermediates and target compounds were characterized and confirmed by nuclear magnetic resonance (NMR) spectroscopy and mass spectrometry (MS) technology.

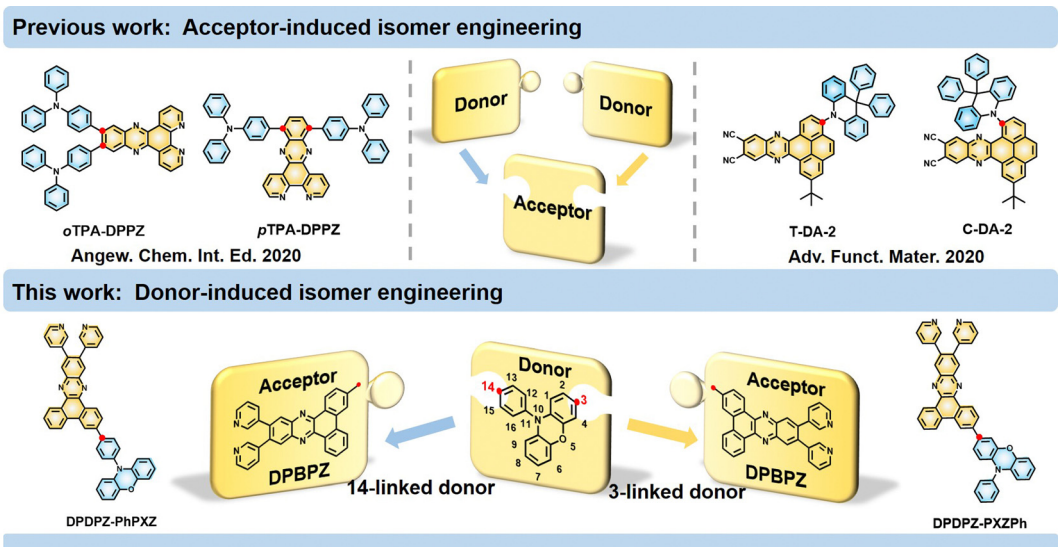

Fig. 1 Molecular design strategies and the chemical structures of materials.

Thermal analysis and electrochemical properties

The thermal stability of both compounds was first assessed using thermogravimetric analysis (TGA) and differential scanning calorimetry (DSC) measurements in a nitrogen atmosphere. As shown in Fig. S1 (ESI†), DPDPZ-PXZPh and DPDPZ-PhPXZ both exhibit sufficiently high decomposition temperatures (T_d, corresponding to 5% weight loss) of 481 and 449 °C, respectively. Additionally, there is no indication of glass transitions for either compound when gradually increasing the testing temperature below 300 °C (Fig. S2, ESI†). These high thermal stabilities support these emitters for the vapor deposition process that is required for device fabrication.

Cyclic voltammetry (CV) measurements were then carried out to investigate their HOMO/LUMO energy levels (Fig. S5, ESI†). As listed in Table 1, based on the onsets of oxidation curves, the HOMO energy levels are estimated to be −5.25 eV for DPDPZ-PXZPh and −5.26 eV for DPDPZ-PhPXZ, respectively. Likewise, from those of their reduction curves, the LUMO energy levels are calculated to be −3.60 and −3.59 eV, respectively. Their nearly identical HOMO and LUMO energy levels indicate that the regioisomerism has a negligible effect on their band gaps.

Theoretical calculations

To explore the influence of regioisomerism on their electronic cloud distributions, theoretical calculations were carried out on these two regioisomers by using density functional theory (DFT) based on the B3LYP/6-31G method. Fig. 2 depicts their optimized geometries in the ground (S_0) state. For either compound, the PXZ group and the free rotated phenyl ring inside the PhPXZ component naturally form a nearly vertical torsion, resulting in minimal π-conjugation. Meanwhile, the torsion values between DPDPZ and PhPXZ components are also very similar to be *ca.* 35°. However, due to their different linking modes, they eventually exhibit distinctly different frontier molecular orbital (FMO) overlaps. As shown in Fig. 2, for both compounds, the LUMOs are dominantly distributed on the DPBPZ units, while their HOMO delocalizations exhibit distinct differences. In DPDPZ-PhPXZ, the HOMO distribution is fully located on the D segment, ensuring the near absence of the HOMO–LUMO overlap, while for DPDPZ-PXZPh, its HOMO is not only distributed on the PXZ moiety but also partially expanded to the DPBPZ framework, resulting in a moderate HOMO–LUMO overlap. As a result, DPDPZ-PXZPh is predicted to have a substantially higher f (0.1680) than DPDPZ-PhPXZ (0.0001), which is favorable for achieving a higher k_r. Natural transition orbital (NTO) analyses were further carried out using time-dependent DFT (TD-DFT) to uncover the characteristics of their excited states. In their lowest singlet (S_1) and triplet (T_1) excited states, holes and particles are clearly separated, mainly

Table 1 Summary of photophysical and electrochemical properties

Compounds	λ_{em}[a]/λ_{em}[b] [nm]	HOMO[c] [eV]	LUMO[d] [eV]	S_1[e]/T_1[e]/ ΔE_{ST}[e] [eV]	Φ_{PL}[f] [%]
DPDPZ-PXZPh	569/598	−5.25	−3.60	2.39/2.27/0.12	95
DPDPZ-PhPXZ	566/578	−5.26	−3.59	2.43/2.36/0.07	68

[a] Determined from the emission maxima of 10^{-5} M toluene solution at R.T. [b] Determined from the emission maxima of DPDPZ-PXZPh (7 wt%) and DPDPZ-PhPXZ (7 wt%) doped in CBP thin films at R.T. [c] Estimated from the onset of the oxidation curves. [d] Estimated from the onset of the reduction curves. [e] Estimated from the onsets of fluorescence and phosphorescence spectra of 7 wt% doped films in the CBP host at 77 K, $\Delta E_{ST} = S_1 - T_1$. [f] Determined from 7 wt% doped films in the CBP host.

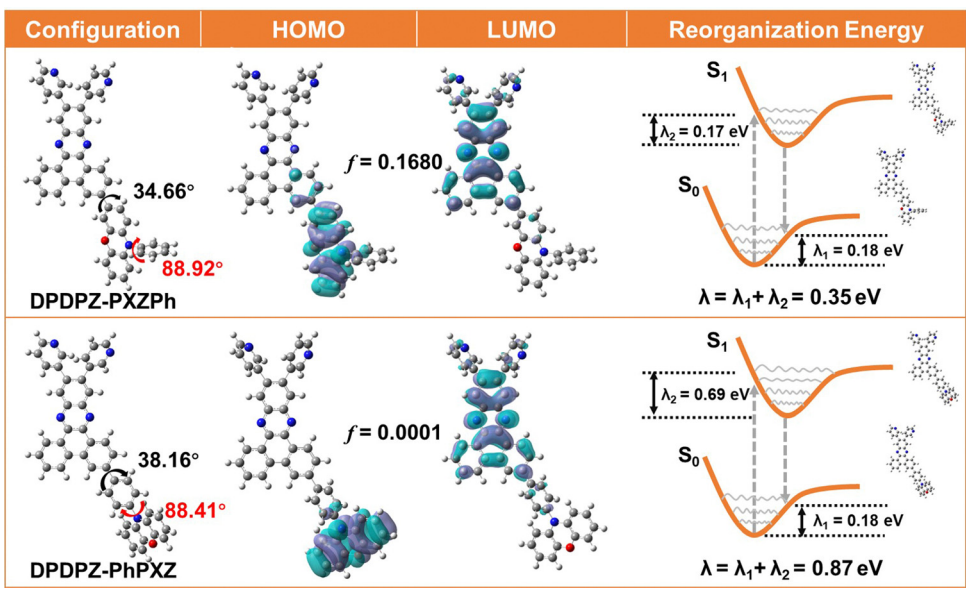

Fig. 2 Molecular configurations and frontier molecular orbital distributions (FMOs) of DPDPZ-PXZPh and DPDPZ-PhPXZ, and their reorganization energies (λ_{ex}) between the S_0 and S_1 states.

on the D and A segments, respectively, clearly indicating their charge-transfer (CT) features. Their geometry changes between the S_0 and S_1 states and the corresponding reorganization energies (λ_{ex}) are depicted in Fig. 2. It is worth noting that the λ_{ex} of DPDPZ-PXZPh is 0.35 eV, evidently lower than that of DPDPZ-PhPXZ (0.87 eV), suggesting that its molecular relaxation could be evidently suppressed *via* such a simple regioisomeric approach.

Photophysical properties

To explore the influences of the regioisomeric approach on their photophysical properties at the single molecule level, ultraviolet-visible (UV-Vis) absorption and PL spectra of DPDPZ-PXZPh and DPDPZ-PhPXZ are first measured in dilute toluene solutions. As shown in Fig. 3a, for both compounds, strong absorption bands before 420 nm are observed, associated with the local π–π* transitions. In the range of *ca.* 420–520 nm, corresponding to the intramolecular CT transitions from D to A components, DPDPZ-PXZPh shows a far stronger intensity than DPDPZ-PhPXZ, which is consistent with their distinctly different *f* values. In terms of their PL spectra, noticeably, both compounds exhibit broad and structureless bands with very close peaks at 569 nm for DPDPZ-PXZPh and 566 nm for DPDPZ-PhPXZ, respectively, in line with their similar band gaps determined from the CV measurement, while the bandwidth of DPDPZ-PXZPh is noticed to be narrower than that of DPDPZ-PhPXZ, which can be ascribed to its smaller λ_{ex} value. We further measured their PL spectra in other solvents with different polarities. As illustrated in Fig. S7 (ESI†), as the solvent environment changes from non-polar (hexane) to highly polar (dioxane), their PL spectra both demonstrate significant solvatochromic redshifts, indicating that both emitters process obvious intramolecular CT natures.

To further investigate the influence of the regioisomerism on their photophysics under host–guest conditions, we then prepared amorphous films of DPDPZ-PXZPh and DPDPZ-PhPXZ 7 wt% doped in 4,4′-bis(9-carbazolyl)-1,1′-biphenyl (CBP). Fig. 3a shows their PL spectra at room temperature. Both films display obvious bathochromic shifts compared to those in dilute solution due to their stronger intermolecular interactions, which are often noticed in red TADF emitters.[36] Notably, the DPDPZ-PXZPh-based film shows an evidently redder emission peaking at 598 nm compared to DPDPZ-PhPXZ (578 nm) under the same conditions, suggesting even stronger interchromophore interactions. By further measuring the fluorescence and phosphorescence spectra of both films at 77 K, the S_1 and T_1 levels are determined to be 2.39 and 2.27 eV for DPDPZ-PXZPh and 2.43 and 2.36 eV for DPDPZ-PhPXZ, respectively. The lower energy levels of DPDPZ-PXZPh in the doped film reveal that it is obviously more stabilized by intermolecular interactions. The ΔE_{ST}s are further calculated to be 0.12 eV for DPDPZ-PXZPh and 0.07 eV for DPDPZ-PhPXZ, respectively (Table 1), supporting their TADF features.

Transient PL decays on these films were measured under oxygen-free conditions at room temperature (Fig. 3b and c). Both

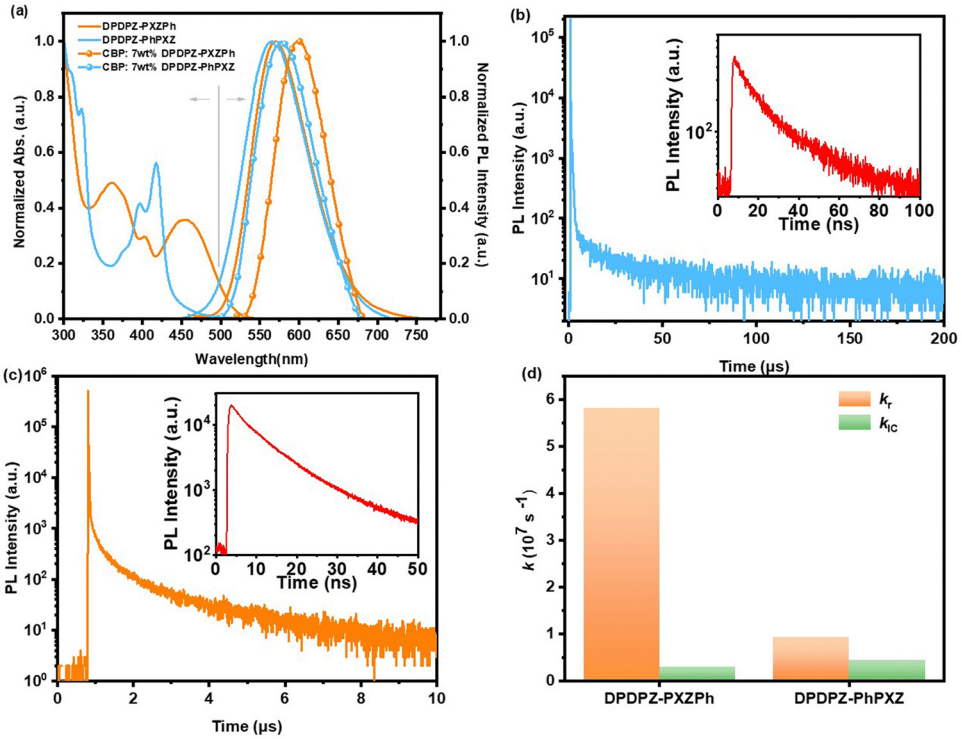

Fig. 3 Photophysical characterizations of DPDPZ-PXZPh and DPDPZ-PhPXZ. (a) Normalized UV-Vis absorption and fluorescence spectra in dilute toluene solutions (1×10^{-5} M) at room temperature and normalized fluorescence spectra doped in a CBP thin film (7 wt%). (b) Transient PL curve of 7 wt% DPDPZ-PhPXZ doped in a CBP thin film (inset: prompt PL decay curve). (c) Transient PL curve of 7 wt% DPDPZ-PXZPh doped in a CBP thin film (inset: prompt PL decay curve). (d) Radiative rates (k_r) and nonradiative rates (k_{IC}) of the two emitters.

regioisomers demonstrate double-exponential decays, revealing their TADF characteristics, while the decay trends are obviously different.[37] The prompt decay lifetimes (τ_p) and delayed lifetimes (τ_d) are evaluated to be 11.64 ns and 397.80 μs for DPDPZ-PXZPh and 32.68 ns and 15.43 μs for DPDPZ-PhPXZ, respectively. Their Φ_{PL}s were evaluated by using an integrating sphere at room temperature. The overall Φ_{PL} is as high as 95% for DPDPZ-PXZPh, substantially higher than that of DPDPZ-PhPXZ (68%), manifesting the higher exciton utilization of DPDPZ-PXZPh. Based on the above results, the key kinetic parameters are further calculated to better understand the structure–performance relationships of this pair of regioisomers. As summarized in Table S1 (ESI†), while both regioisomers exhibit close k_{IC} values of $\sim 4 \times 10^6$ s^{-1}, k_r of DPDPZ-PXZPh is estimated to be 5.81×10^7 s^{-1}, lifting approximately 6.2-fold that of DPDPZ-PhPXZ (0.93×10^7 s^{-1}). The larger k_r value of DPDPZ-PXZPh is due to its enhanced HOMO–LUMO overlap and thus larger f, which is very important for ultimately harvesting excitons (Fig. 3d).

To shed light on the effect of different linking modes at intermolecular levels, single crystals of DPDPZ-PXZPh and DPDPZ-PhPXZ were cultivated from the chloroform/ethyl acetate mixed solution and chloroform/ethanol mixed solution, respectively, and further analyzed *via* X-ray diffraction (XRD) measurements. Fig. 4 depicts the molecular geometries of both regioisomers in the crystal samples. DPDPZ-PhPXZ displays a more obvious torsional conformation than DPDPZ-PXZPh. The flatter geometry of DPDPZ-PXZPh is beneficial for intermolecular π–π interactions, especially in highly disordered conditions (*e.g.*, doped films). Fig. 4 also shows molecular packings in the crystal lattices. It is notable that the peripheral pyridine groups in DPDPZ-PXZPh engage in a pair of C–H···N hydrogen bonds with a distance of 2.578 Å, which is helpful to suppress the nonradiative loss and thus rigidify the overall system, whereas such interactions are not found between DPDPZ-PhPXZ molecules.[38] It is worth noting that although both molecules are arranged in similar "head-to-tail" manners, DPDPZ-PXZPh shows a relatively closer stacking with an interplanar distance of 3.289 Å compared to DPDPZ-PhPXZ (3.457 Å), which supports a redder emission wavelength of DPDPZ-PXZPh under host–guest conditions.[39]

Electroluminescence properties

To explore the effect of the D/A linking modes on electroluminescence (EL) performance, multi-layer OLEDs were fabricated with a configuration of ITO/HATCN (7 nm)/TAPC (35 nm)/TCTA (10 nm)/mCP (10 nm)/emitting layers (EML) (20 nm)/TmPyPB (45 nm)/LiF (1 nm)/Al, where ITO (indium tin oxide) and Al were used as the anode and the cathode, respectively; HATCN (1,4,5,8,9,11-hexaazatriphenylenehexacarbonitrile), TAPC (di[4-(*N*,*N*-ditolyl-amino)-phenyl]cyclohexane), TmPyPB (1,3,5-tri[(3-pyridyl)phen-3-yl]-benzene) and LiF served as the hole-injecting, hole-transporting, electron-transporting and electron-injecting layers, respectively; TCTA (tris(4-(9*H*-carbazol-9-yl)phenyl)amine) and mCP (1,3-bis(*N*-carbazolyl) benzene) both function as exciton blocking layers. In the EML, DPDPZ-PXZPh and DPDPZ-PhPXZ were doped into the CBP host at various doping concentrations in the range of 5–11 wt%. The energy level diagrams of the OLED devices and corresponding used materials are shown in Fig. 5a and Fig. S7a (ESI†). The key EL performances of all these devices are summarized in Table 2.

As displayed in Table 2, at each doping level, the DPDPZ-PXZPh-based OLED exhibits a slightly redder EL spectrum in

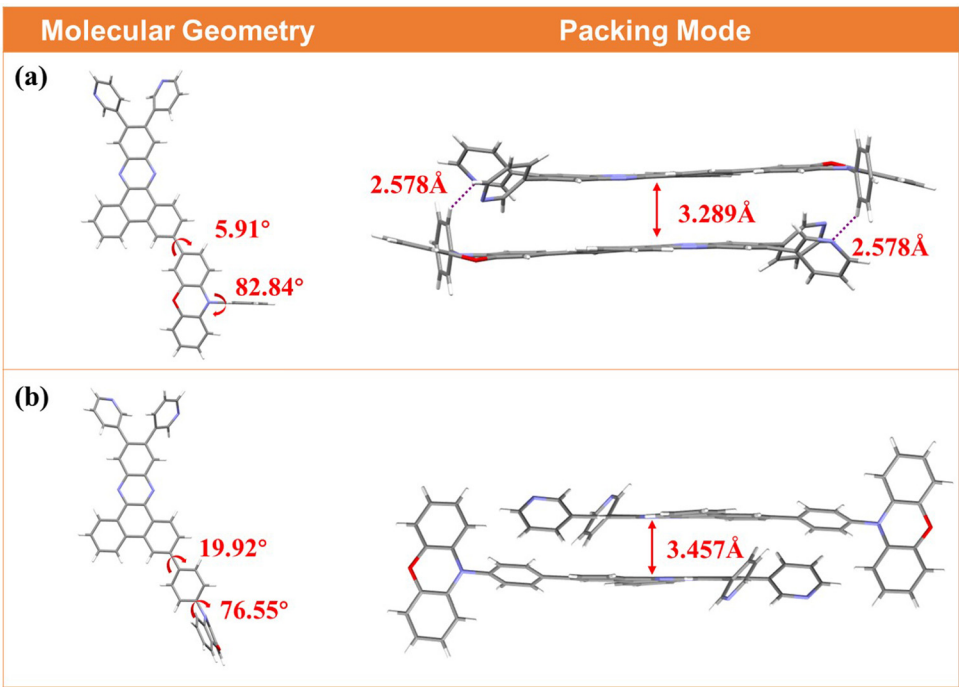

Fig. 4 Molecular geometries and packing modes of (a) DPDPZ-PXZPh and (b) DPDPZ-PhPXZ in single crystals.

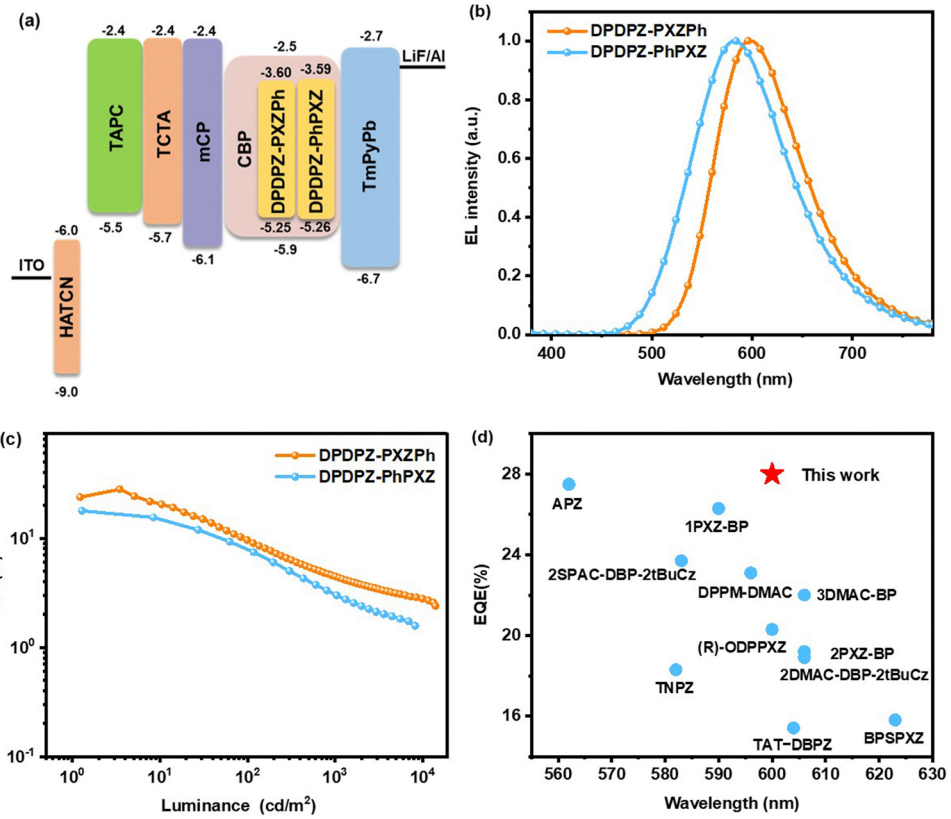

Fig. 5 EL performances of DPDPZ-PXZPh- and DPDPZ-PhPXZ-based OLEDs. (a) The configuration of OLED devices. (b) EL spectra at the optimized doping concentrations. (c) EQE *versus* luminance curves. (d) EQE summary of TADF materials based on the dibenzo[*a*,*c*]phenazine backbone with EL spectral peaks in the range of 560–630 nm (see Table S2 for details, ESI†).

Table 2 Summary of device performances of DPDPZ-PXZPh- and DPDPZ-PhPXZ-based OLEDs at various doping concentrations

Emitters	Conc. (wt%)	Peak (nm)	CE_{max} (cd A^{-1})	PE_{max} (lm W^{-1})	EQE_{max} (%)	CIE (x, y)
DPDPZ-PXZPh	5	592	56.5	52.2	25.1	(0.54, 0.44)
	7	600	54.4	40.7	28.0	(0.57, 0.43)
	9	604	42.5	38.2	23.8	(0.58, 0.42)
	11	608	37.4	35.6	21.6	(0.60, 0.40)
DPDPZ-PhPXZ	5	580	42.9	34.6	16.2	(0.49, 0.47)
	7	584	47.9	45.6	17.8	(0.51, 0.48)
	9	588	41.1	39.1	16.8	(0.52, 0.47)
	11	592	34.7	33.0	14.5	(0.53, 0.46)

the range of 592–608 nm relative to the corresponding DPDPZ-PhPXZ-based OLED (580–592 nm), which is in line with their film PL results. Inspiringly, the 7 wt% DPDPZ-PXZPh-doped device achieves a red EL emission peaking at 600 nm and reaches the best performance with a maximum EQE of 28.0%, maximum current efficiency (CE) of 54.4 cd A^{-1} and maximum power efficiency (PE) of 40.7 lm W^{-1} (Fig. 5b and c). Such device performance is not only evidently superior to that of the DPDPZ-PhPXZ-based device (EQE = 17.8%, CE = 47.9 cd A^{-1}, and PE = 45.6 lm W^{-1}) but also an outstanding result among TADF emitters taking the dibenzo[*a*,*c*]-phenazine moiety as the A main body with emission peaks between 560 and 630 nm (Fig. 5d). A larger k_r, smaller k_{IC}, and higher Φ_{PL} of DPDPZ-PXZPh, which all result from its better D–A linking mode, are responsible for its much-improved EL efficiencies, further validating the effectivity of the regioisomeric approach from the D side.

Conclusions

In summary, we designed and synthesized two regioisomeric red TADF emitters, DPDPZ-PXZPh and DPDPZ-PhPXZ, by manipulating the linking sites in terms of the D segment. DPDPZ-PXZPh with the 3-position connected PhPXZ group features a milder D–A linking mode, exhibiting a higher f and lower reorganization energies relative to the control compound DPDPZ-PhPXZ with a conventional 14-position connected PhPXZ. As a result, DPDPZ-PXZPh offers a higher k_r, which shows overwhelming superiority over the k_{IC}, thus bringing about a much-improved Φ_{PL} of 95% with respect to DPDPZ-PhPXZ. Correspondingly, the optimized DPDPZ-PXZPh-based OLED realizes a redder EL performance peaking at 600 nm and a superior EQE of 28.0%, presenting the highest value among ever-reported TADF emitters containing

dibenzo[*a*,*c*]phenazine A fragments thus far. This work highlights the potential of managing D connecting patterns for constructing high-efficiency red TADF emitters, providing a straightforward strategy for developing highly efficient red OLED emitters from the aspect of D regioisomerism.

Author contributions

The manuscript was written through contributions of all authors. Xi Zhang: writing – original draft, validation, formal analysis, visualization, and software; Hui Wang: conceptualization, methodology, writing – review and editing, and visualization; Jia-Xiong Chen: conceptualization, supervision; Lu Zhou: software, data curation; Xiao-Yao Hao: data curation; Jia Yu, review; and Kai Wang and Xiao-Hong Zhang: writing – review and editing, funding acquisition, resources, supervision, and project administration. All authors have given approval to the final version of the manuscript.

Conflicts of interest

There are no conflicts to declare.

Acknowledgements

This work was supported by the National Natural Science Foundation of China (Grant No. 52130304, 51821002, 52003185, 52003187, and 52373193), the National Key Research & Development Program of China (Grant No. 2020YFA0714601, 2020YFA0714604), the Science and Technology Program of Suzhou (Grant No. ZXL2022490), the National Science and Technology Program of the Ministry of Science and Technology of China (Grant No. G2022030035L), Postgraduate Research & Practice Innovation Program of Jiangsu Province (Grant No. KYCX23_3244), Suzhou Key Laboratory of Functional Nano & Soft Materials, Collaborative Innovation Center of Suzhou Nano Science & Technology, the 111 Project, and Joint International Research Laboratory of Carbon-Based Functional Materials and Devices.

References

1 H. Uoyama, K. Goushi, K. Shizu, H. Nomura and C. Adachi, Highly Efficient Organic Light-Emitting Diodes from Delayed Fluorescence, *Nature*, 2012, **492**, 234–238.
2 T. L. Wu, M. J. Huang, C. C. Lin, P. Y. Huang, T. Y. Chou, R. W. Chen-Cheng, H. W. Lin, R. S. Liu and C. H. Cheng, Diboron Compound-Based Organic Light-Emitting Diodes with High Efficiency and Reduced Efficiency Roll-Off, *Nat. Photon.*, 2018, **12**, 235–240.
3 S. Wang, X. Yan, Z. Cheng, H. Zhang, Y. Liu and Y. Wang, Highly Efficient Near-Infrared Delayed Fluorescence Organic Light Emitting Diodes Using a Phenanthrene-Based Charge-Transfer Compound, *Angew. Chem., Int. Ed.*, 2015, **54**, 13068–13072.
4 G. Hong, X. Gan, C. Leonhardt, Z. Zhang, J. Seibert, J. M. Busch and S. Brase, A Brief History of OLEDs-Emitter Development and Industry Milestones, *Adv. Mater.*, 2021, **33**, e2005630.
5 M. Y. Wong and E. Zysman-Colman, Purely Organic Thermally Activated Delayed Fluorescence Materials for Organic Light-Emitting Diodes, *Adv. Mater.*, 2017, **29**, 1605444.
6 Y. Im, M. Kim, Y. J. Cho, J. A. Seo, K. S. Yook and J. Y. Lee, Molecular Design Strategy of Organic Thermally Activated Delayed Fluorescence Emitters, *Chem. Mater.*, 2017, **29**, 1946–1963.
7 S. Park, S. Y. Lee, C. Adachi and T. Yasuda, Full-Color Delayed Fluorescence Materials Based on Wedge-Shaped Phthalonitriles and Dicyanopyrazines: Systematic Design, Tunable Photophysical Properties, and OLED Performance, *Adv. Funct. Mater.*, 2016, **26**, 1813–1821.
8 J. F. Cheng, Z. H. Pan, K. Zhang, Y. Zhao, C. K. Wang, L. Ding, M. K. Fung and J. Fan, High-Performance Solution-Processed Red Thermally Activated Delayed Fluorescence OLEDs Employing Aggregation-Induced Emission-Active Triazatruxene-Based Emitters, *ACS Appl. Mater. Interfaces*, 2020, **12**, 30652–30658.
9 S. Kothavale, W. J. Chung and J. Y. Lee, Rational Molecular Design of Highly Efficient Yellow-Red Thermally Activated Delayed Fluorescent Emitters: A Combined Effect of Auxiliary Fluorine and Rigidified Acceptor Unit, *ACS Appl. Mater. Interfaces*, 2020, **12**, 18730–18738.
10 J. X. Chen, W.-W. Tao, W. C. Chen, Y. F. Xiao, K. Wang, C. Cao, J. Yu, S. Li, F. X. Geng, C. Adachi, C. S. Lee and X. H. Zhang, Red/Near-Infrared Thermally Activated Delayed Fluorescence OLEDs with Near 100% Internal Quantum Efficiency, *Angew. Chem., Int. Ed.*, 2019, **58**, 14660–14665.
11 Q. Zhang, H. Kuwabara, W. J. Potscavage, Jr., S. Huang, Y. Hatae, T. Shibata and C. Adachi, Anthraquinone-Based Intramolecular Charge-Transfer Compounds: Computational Molecular Design, Thermally Activated Delayed Fluorescence, and Highly Efficient Red Electroluminescence, *J. Am. Chem. Soc.*, 2014, **136**, 18070–18081.
12 J. V. Caspar, E. M. Kober, B. P. Sullivan and T. J. Meyer, Application of the Energy Gap Law to the Decay of Charge-Transfer Excited States, *J. Am. Chem. Soc.*, 1982, **104**, 630–632.
13 Y. Liu, J. Yang, Z. Mao, X. Chen, Z. Yang, X. Ge, X. Peng, J. Zhao, S. J. Su and Z. Chi, Asymmetric Thermally Activated Delayed Fluorescence Emitter for Highly Efficient Red/Near-Infrared Organic Light-Emitting Diodes, *ACS Appl. Mater. Interfaces*, 2022, **14**, 33606–33613.
14 J. X. Chen, K. Wang, C. J. Zheng, M. Zhang, Y. Z. Shi, S. L. Tao, H. Lin, W. Liu, W. W. Tao, X. M. Ou and X. H. Zhang, Red Organic Light-Emitting Diode with External Quantum Efficiency Beyond 20% Based on a Novel Thermally Activated Delayed Fluorescence Emitter, *Adv. Sci.*, 2018, **5**, 1800436.
15 Y. H. He, F. M. Xie, K. Zhang, D. Yang, Y. Shen, H. Z. Li, D. Ma, Y. Q. Li and J. X. Tang, Acceptor-Donor-Acceptor-Configured Delayed Fluorescence Emitters for Efficient Orange-Red and White Devices with Low Roll-off, *Adv. Funct. Mater.*, 2023, **33**, 2304006.
16 R. Furue, K. Matsuo, Y. Ashikari, H. Ooka, N. Amanokura and T. Yasuda, Highly Efficient Red-Orange Delayed Fluorescence Emitters Based on Strong Π-Accepting Dibenzophenazine

and Dibenzoquinoxaline Cores: Toward a Rational Pure-Red OLED Design, *Adv. Opt. Mater.*, 2018, **6**, 1701147.

17 L. Zhou, H. Wang, Y. Z. Shi, X. C. Fan, J. X. Chen, K. Wang, J. Yu and X. H. Zhang, Controlling the Conjugation Extension inside Acceptors for Enhancing Reverse Intersystem Crossing of Red Thermally Activated Delayed Fluorescence Emitters, *Chem. Eng. J.*, 2022, **440**, 135775.

18 H. Wang, L. Zhou, Y. Z. Shi, X. C. Fan, J. X. Chen, K. Wang, J. Yu and X. H. Zhang, A Facile Strategy for Enhancing Reverse Intersystem Crossing of Red Thermally Activated Delayed Fluorescence Emitters, *Chem. Eng. J.*, 2022, **433**, 134423.

19 S. Kothavale, W. J. Chung and J. Y. Lee, High Efficiency and Long Lifetime Orange-Red Thermally Activated Delayed Fluorescent Organic Light Emitting Diodes by Donor and Acceptor Engineering, *J. Mater. Chem. C*, 2021, **9**, 528–536.

20 C. Li, R. Duan, B. Liang, G. Han, S. Wang, K. Ye, Y. Liu, Y. Yi and Y. Wang, Deep-Red to Near-Infrared Thermally Activated Delayed Fluorescence in Organic Solid Films and Electroluminescent Devices, *Angew. Chem., Int. Ed.*, 2017, **56**, 11525–11529.

21 Z. Yang, Z. Mao, Z. Xie, Y. Zhang, S. Liu, J. Zhao, J. Xu, Z. Chi and M. P. Aldred, Recent Advances in Organic Thermally Activated Delayed Fluorescence Materials, *Chem. Soc. Rev.*, 2017, **46**, 915–1016.

22 D. Zhang, X. Song, M. Cai, H. Kaji and L. Duan, Versatile Indolocarbazole-Isomer Derivatives as Highly Emissive Emitters and Ideal Hosts for Thermally Activated Delayed Fluorescent OLEDs with Alleviated Efficiency Roll-Off, *Adv. Mater.*, 2018, **30**, 1705406.

23 D. Zhang, Y. Wada, Q. Wang, H. Dai, T. Fan, G. Meng, J. Wei, Y. Zhang, K. Suzuki, G. Li, L. Duan and H. Kaji, Highly Efficient and Stable Blue Organic Light-Emitting Diodes Based on Thermally Activated Delayed Fluorophor with Donor-Void-Acceptor Motif, *Adv. Sci.*, 2022, **9**, e2106018.

24 Y. Li, X. L. Li, D. Chen, X. Cai, G. Xie, Z. He, Y. C. Wu, A. Lien, Y. Cao and S. J. Su, Design Strategy of Blue and Yellow Thermally Activated Delayed Fluorescence Emitters and Their All-Fluorescence White OLEDs with External Quantum Efficiency Beyond 20%, *Adv. Funct. Mater.*, 2016, **26**, 6904–6912.

25 J. Li, L. Zhou, J. He, Q. Xue, L. Xu and G. Xie, Propeller-Shape Isomers with Turn-on Through-Space Charge Transfer for Solution-Processed Non-Doped Organic Light-Emitting Diodes, *Chem. Eng. J.*, 2023, **452**, 139120.

26 C. Zhou, W. C. Chen, H. Liu, X. Cao, N. Li, Y. Zhang, C. S. Lee and C. Yang, Isomerization Enhanced Quantum Yield of Dibenzo[*a*,*c*]Phenazine-Based Thermally Activated Delayed Fluorescence Emitters for Highly Efficient Orange OLEDs, *J. Mater. Chem. C*, 2020, **8**, 9639–9645.

27 A. Shang, T. Lu, H. Liu, C. Du, F. Liu, D. Jiang, J. Min, H. Zhang and P. Lu, Study of Configuration Differentia and Highly Efficient Deep-Red Thermally Activated Delayed Fluorescent Organic Light-Emitting Diodes Based on Phenanthro[4,5-*fgh*]Quinoxaline Derivatives, *J. Mater. Chem. C*, 2021, **9**, 7392–7399.

28 T. Yang, J. Liang, Y. Cui, Z. Li, X. Peng, S. J. Su, Y. Wang and C. Li, Achieving 34.3% External Quantum Efficiency for Red Thermally Activated Delayed Fluorescence Organic Light-Emitting Diode by Molecular Isomer Engineering, *Adv. Opt. Mater.*, 2022, **11**, 2201191.

29 B. Zhao, H. Wang, C. Han, P. Ma, Z. Li, P. Chang and H. Xu, Highly Efficient Deep-Red Non-Doped Diodes Based on a T-Shape Thermally Activated Delayed Fluorescence Emitter, *Angew. Chem., Int. Ed.*, 2020, **59**, 19042–19047.

30 T. Yang, Z. Cheng, Z. Li, J. Liang, Y. Xu, C. Li and Y. Wang, Improving the Efficiency of Red Thermally Activated Delayed Fluorescence Organic Light-Emitting Diode by Rational Isomer Engineering, *Adv. Funct. Mater.*, 2020, **30**, 2002681.

31 Y. Liu, J. Yang, Z. Mao, Y. Wang, J. Zhao, S. J. Su and Z. Chi, Isomeric Thermally Activated Delayed Fluorescence Emitters for Highly Efficient Organic Light-Emitting Diodes, *Chem. Sci.*, 2023, **14**, 1551–1556.

32 H. Wang, J. X. Chen, X. C. Fan, Y. C. Cheng, L. Zhou, X. Zhang, J. Yu, K. Wang and X. H. Zhang, A TADF Emitter with Dual Para-Positioned Donors Enables OLEDs with Improved Efficiency and CIE Coordinates Close to the Rec. 2020 Red Standard, *ACS Appl. Mater. Interfaces*, 2023, **15**, 1685–1692.

33 J. X. Chen, W. W. Tao, Y. F. Xiao, S. Tian, W. C. Chen, K. Wang, J. Yu, F. X. Geng, X. H. Zhang and C. S. Lee, Isomeric Thermally Activated Delayed Fluorescence Emitters Based on Indolo[2,3-*b*]Acridine Electron-Donor: A Compromising Optimization for Efficient Orange–Red Organic Light-Emitting Diodes, *J. Mater. Chem. C*, 2019, **7**, 2898–2904.

34 J. X. Chen, Y. F. Xiao, K. Wang, D. Sun, X. C. Fan, X. Zhang, M. Zhang, Y. Z. Shi, J. Yu, F. X. Geng, C. S. Lee and X. H. Zhang, Managing Locally Excited and Charge-Transfer Triplet States to Facilitate Up-Conversion in Red TADF Emitters That Are Available for Both Vacuum- and Solution-Processes, *Angew. Chem., Int. Ed.*, 2021, **60**, 2478–2484.

35 U. Balijapalli, Y. T. Lee, B. S. B. Karunathilaka, G. Tumen-Ulzii, M. Auffray, Y. Tsuchiya, H. Nakanotani and C. Adachi, Tetrabenzo[*a*,*c*]Phenazine Backbone for Highly Efficient Orange-Red Thermally Activated Delayed Fluorescence with Completely Horizontal Molecular Orientation, *Angew. Chem., Int. Ed.*, 2021, **60**, 19364–19373.

36 J. Xue, Q. Liang, R. Wang, J. Hou, W. Li, Q. Peng, Z. Shuai and J. Qiao, Highly Efficient Thermally Activated Delayed Fluorescence Via J-Aggregates with Strong Intermolecular Charge Transfer, *Adv. Mater.*, 2019, **31**, e1808242.

37 S. Kothavale, K. H. Lee and J. Y. Lee, Isomeric Quinoxaline-dicarbonitrile as Color-Managing Acceptors of Thermally Activated Delayed Fluorescent Emitters, *ACS Appl. Mater. Interfaces*, 2019, **11**, 17583–17591.

38 Z. Cai, X. Wu, H. Liu, J. Guo, D. Yang, D. Ma, Z. Zhao and B. Z. Tang, Realizing Record-High Electroluminescence Efficiency of 31.5% for Red Thermally Activated Delayed Fluorescence Molecules, *Angew. Chem., Int. Ed.*, 2021, **60**, 23635–23640.

39 S. K. Mohan Nalluri, J. Zhou, T. Cheng, Z. Liu, M. T. Nguyen, T. Chen, H. A. Patel, M. D. Krzyaniak, W. A. Goddard III, M. R. Wasielewski and J. F. Stoddart, Discrete Dimers of Redox-Active and Fluorescent Perylene Diimide-Based Rigid Isosceles Triangles in the Solid State, *J. Am. Chem. Soc.*, 2019, **141**, 1290–1303.